Effect of Dissolved Oxygen Concentration on Dynamic Strain Aging and Stress Corrosion Cracking of SUS304 Stainless Steel under High Temperature Pressurized Water

Noriaki Hirota[1,3, a)], Hiroko Nakano[1], Yoshitaka Fujita[1], Tomoaki Takeuchi[1], Kunihiko Tsuchiya[1], Masahiko Demura[2] and Yoshinao Kobayashi[3]

[1]*Japan Atomic Energy Agency, 4002, Narita, Oarai, Higashiibaraki, Ibaraki 311-1393, Japan.*
[2] *National Institute for Materials Science, 1-1, Namiki, Tsukuba, Ibaraki, 305-0044, Japan.*
[3]*Tokyo Institute of Technology, 2-12-1, Ookayama, Meguro-ku, Tokyo, 152-8550, Japan.*

[a)] *Corresponding author: hirota.noriaki@jaea.go.jp*

Keywords: Dissolved oxygen; Dynamic strain aging; Stress corrosion cracking; oxide film

Abstract. Under high temperature pressurized water assuming the interior of a typical nuclear reactor, dynamic strain aging (DSA) and intergranular stress corrosion cracking (intragranular SCC) occur due to changes in dissolved oxygen (DO) content, respectively. In order to clearly understand the difference between these phenomena, the mechanism of their occurrence was summarized. As a result, DSA due to intragranular cracking was found to occur in AISI 304 stainless steel at low DO < 1 ppb and 100 ppb, while DSA was suppressed at DO 8500 ppb due to the formation of oxide films on the surface. On the other hand, when DO was increased to 20000 ppb, the film was peeled from the matrix, O element diffused to the grain boundary of the matrix, resulting in intergranular SCC. These results are indicated that the optimum DO concentration should be adjusted to suppress crack initiation due to DSA and intergranular SCC.

1. INTRODUCTION

Stress corrosion cracking (SCC) has been identified near the weld heat-affected zone (HAZ) in the shrouds of boiling water reactor (BWR) and in the recirculation system piping of pressurized water reactor (PWR), and many studies have been implemented to elucidate the mechanisms involved in maintaining the reliability of nuclear power plants [1]. Material composition, environment, and tensile residual stress is considered to be the main contributors to the occurrence of SCC. Regarding the material composition, the formation of Cr-deficient phase, which makes the grain boundary brittle, is a problem in AISI 304 (SUS304) and 316 stainless steels [2]. From the environmental point of view, intergranular SCC and crack propagation occurs due to the increase of dissolved oxygen (DO) content under high temperature pressurized water [3,4]. From the stress point of view, tensile stress on the surface of the matrix, especially in the vicinity of HAZ, is thought to be a factor. It has been reported that the material hardening near the HAZ is due to tensile deformation caused by the solidification and shrinkage of the metal in the HAZ. Therefore, one of the factors contributing to the hardening of the HAZ is the occurrence of dynamic strain aging (DSA) during high-temperature deformation [5]. DSA is a phenomenon in which, unlike SCC, the nominal stress-nominal strain curve (S-S curve) shows a serrated shape when the material is subjected to the interaction of solute atoms and segregation into dislocations. On the other hand, there is no clear definition of the fracture modes of DSA and intergranular SCC, as they are sometimes mistakenly thought to be the same phenomenon and are difficult to distinguish due to differences in microstructure. Therefore, the purpose of this study is to clearly understand how DSA and intergranular SCC are formed by changes in DO content in a high temperature pressurized water simulating nuclear reactor environment.

2. EXPERIMENTAL PROCEDURE

2.1. Test specimen

SUS304 stainless steel was utilized as the specimen material. After forming the plate by rolling, solution annealing was performed at 1050 °C for 2h and water quenched. The grain size of the material was measured by a cutting method. As a result, the grain size was confirmed to be 25 μm ± 5 μm and well-grained. The material was cut into bars, and the bars were formed into tensile specimens along the rolling direction. The tensile specimen had a gauge distance of 16 mm, a thickness and width of 2 mm, and a length of 44 mm.

2.2. Tensile testing

A slow strain rate testing (SSRT) was conducted in air with strain rate of 5.2×10^{-6} s^{-1} at 325 °C to evaluate tensile properties in a PWR environment, which is assumed to the interior of a typical nuclear reactor. In this SSRT, a marker was placed on the specimen in the gauge direction, and the amount of elongation change in the elastic range at elevated temperatures was measured using a laser displacement meter. On the other hand, to reproduce the DSA and SCC phenomenon, an autoclave unit was fabricated and SSRT was conducted using a high-temperature, high-pressure water loop [6]. A PWR environment at 325 °C and 15 MPa was created under pure water as tensile conditions, and the S-S curves were obtained at a strain rate of 5.2×10^{-6} s^{-1} as in the previous case. The DO in the water was intentionally varied from < 1 ppb to 20 ppm by monitoring the DO meter.

2.3. Microstructure analysis

The fracture zone after SSRT was observed by Field Emission Scanning Electron Microscopy to evaluate the fracture mode and ratio of brittle fracture. And Electron Backscattered Diffraction pattern (EBSD) was utilized to analyze the crystal orientation distribution and precipitation phase. Furthermore, the thickness of the oxide film and elemental distribution in each area were determined by Field Emission Electron Probe Micro Analysis near the surface of the fracture. X-ray Photoelectron Spectroscopy (XPS) was utilized to analyze the oxide structure at the surface layer.

3. RESULTS

3.1. Mechanical properties in air and stress-strain curve under high temperature pressurized water with change in DO

In the SSRT at 325 °C in air, the elastic modulus measured with a laser displacement meter was 170 GPa. Although nominal stress-nominal strain curve was not shown, the 0.2% yield stress was 223 MPa and the tensile strength was 602 MPa. And the fracture strain value was 0.53, confirming to be similar to the value of ductility observed in general SUS304. Figure 1 (a) shows the nominal stress-nominal strain curves after SSRT for a step change in DO under high temperature pressurized water. Incidentally, the data for DO < 1 ppb and 8500 ppb were obtained by Takeuchi et al. [7]. The fracture strain at DO < 1 ppb was significantly reduced compared to the strain value at SSRT in air, whereas both DO 100 ppb and 8500 ppb showed close to the strain value in air. On the other hand, under DO 20000 ppb, the specimen had the lowest fracture strain of 0.23 and the lowest tensile strength of 453 MPa compared to the other specimens. Figure 1 (b) shows an enlarged view of Figure 1 (a). At DO < 1 ppb and 100 ppb, serration from the elastic region to rupture was observed by the brown and blue line. On the other hand, at DO 8500 ppb, the serration was considerably suppressed as indicated by the red line, and at DO 20000 ppb, the amplitude of serration was also small as indicated by the green line. In particular, the stress increase for a strain range of 0.0003 at DO < 1 ppb and 100 ppb was about 18 MPa, whereas at DO 20000 ppb, the stress increase was slightly lower at about 9 MPa for the same strain range. This result is indicated that DSA may be occurring at DO <1 ppb and 100 ppb when the stress increase is as large as 18 MPa. In fact, in the reference [5], differences in stress amplitude widths were observed for certain range of temperature conditions and strain rates, and it is assumed that the changes in this study were caused by differences in the amount of DO.

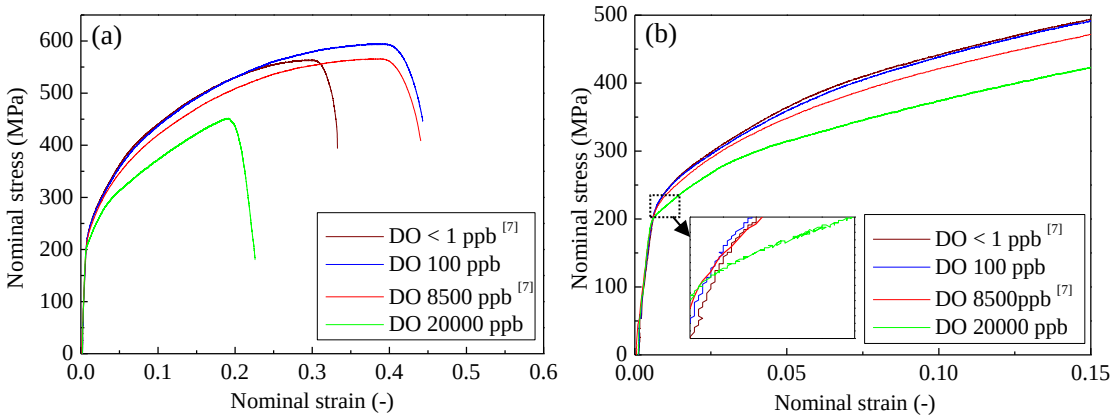

FIGURE 1. (a) Nominal stress-nominal strain curves after SSRT for a step change in DO under high temperature pressurized water, (b) Enlarged view of Figure 1 (a).

3.2. Microstructure observation in the vicinity of fracture after SSRT

Figure 2 shows the results of overview observation from just above the fracture surface and from the side and enlarged view, misorientation angle (MA) and inverse pole figure (IPF) image after SSRT under high temperature pressurized water at DO < 1ppb, 8500 ppb, and 20000 ppb. The view at DO < 1 ppb shows a ductile fracture surface near the center, but a brittle fracture surface at the periphery, indicated by the red dotted line (Figure 2 (a)). On the other hand, at DO 8500 ppb, it can be seen that no brittle fracture surfaces were observed (Figure 2 (f)). However, at an even higher DO 20000 ppb, intergranular SCC was occurred where the entire surface was carved from the grain boundary (Figure 2 (k)). In other words, the fracture morphology at DO <1 ppb is different from intergranular SCC at DO 20000 ppb. Overview observation of the side showed that the largest number of cracks

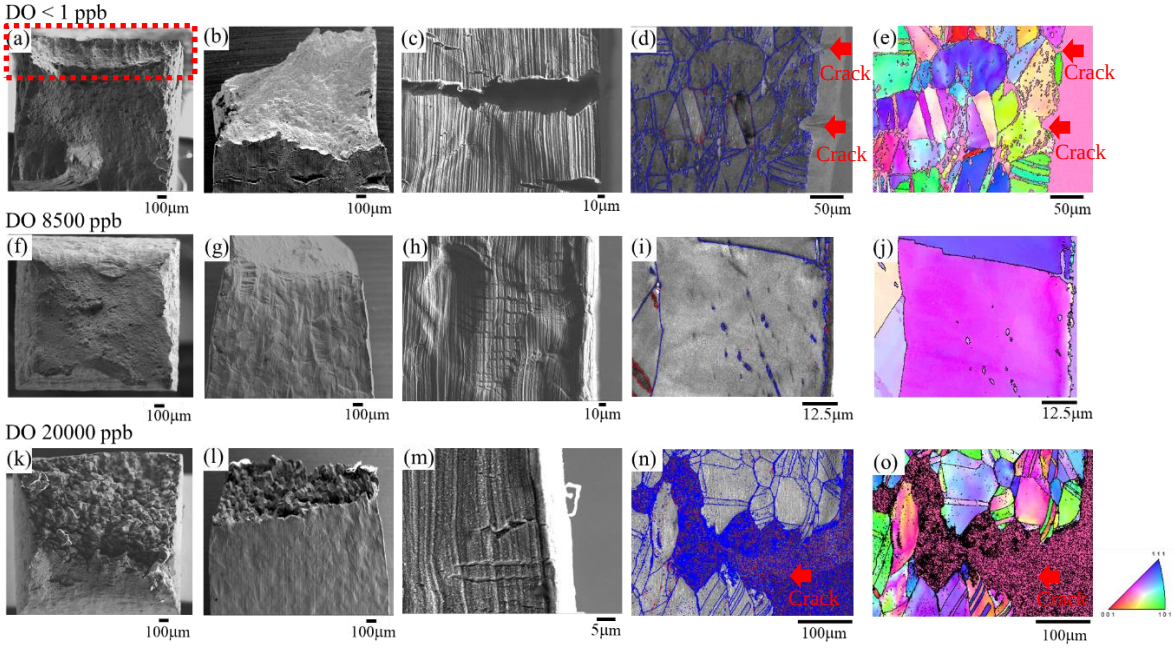

FIGURE 2. Overview observation from just above, side and enlarged view, MA and IPF image near crack by EBSD of tensile fracture cross section after SSRT with DO change under high temperature pressurized water. (a), (b), (c), (d), (e) are under DO < 1ppb, (f), (g), (h), (i), (j) are under DO 8500 ppb, (k), (l), (m), (n), (o) are under DO 20000 ppb. Furthermore, (d), (f), (n) are MA at 5° and 15° (red) and at grain boundaries larger than 15° (blue) and (e), (j), (o) are IPF image.

were existed at DO < 1 ppb (Figure 2 (b), (c)). On the other hand, at DO 8500 ppb and 20000 ppb, there were almost no side cracks (Figure 2 (g), (l)). Nevertheless, enlarged view of the side portions of both showed the existence of cracks in some places ((Figure 2 (h), (m)). This result was consistent with a change in serration shape due to difference in DO, especially under DO < 1 ppb, which the number of cracks was high, and the fracture strain was significantly low as shown in Figure 1. EBSD observations of the MA at low angle boundaries between 5° and 15° (red) and at high angle boundaries larger than 15° (blue) showed that there were almost no low angle boundaries in the vicinity of these cracks (Figure 2 (d), (i), (n)). Okayasu et al. was reported on SUS304 that the formation of α' martensite affected the tensile strength and ductility of the material [8]. In particular, they have also been shown to form α' martensite at MA in the range of 5° to 15°. From the distribution of MA in this study, it can be assumed that at least the crack-induced ductility loss is not caused by α' martensite. This is because no low angle boundaries between 5° to 15° were observed near the cracks at DO < 1 ppb. The IPF images showed that cracks propagated into the grains rather than grain boundaries at DO < 1 ppb (Figure 2 (e)). At DO 8500 ppb, no cracks were observed (Figure 2 (j)). On the other hand, at DO 20000 ppb, where intergranular SCC was observed, cracks propagated mainly at grain boundaries (Figure 2 (o)). The results are indicated that the crack initiation observed in the side view at DO < 1 ppb is DSA due to temporary hardening and softening into the grains. At DO 20000 ppb, intergranular SCC is assumed to have occurred due to grain boundary embrittlement. This grain boundary embrittlement is also assumed to have affected the serration of the stress-strain curve. Furthermore, similar microstructural observations were confirmed by Andresen et al. in CT specimens utilizing SUS316L stainless steel [9].

3.3. Microstructural analysis of oxide film morphology

Figure 3 shows EPMA analysis of each element at the surface in the side of the specimen after SSRT under high temperature pressurized water at DO < 1 ppb, 8500 ppb, and 20000 ppb. At DO < 1 ppb, where many cracks were observed, there was no oxide film at all around the cracks. On the other hand, at DO 8500 ppb, oxide films consisting mainly of Fe and Cr was observed. Furthermore, at DO 20000 ppb, oxide films consisting of Fe, Ni, and Cr were formed on the entire side surface. In particular, these oxide films existed with a gap between them and the matrix and were not observed to adhere closely. This is indicated that the side cracks observed at DO < 1 ppb are not formed by oxide film. On the other hand, when DO increases to 8500 ppb, an oxide film consisting of Fe or Cr is formed on the

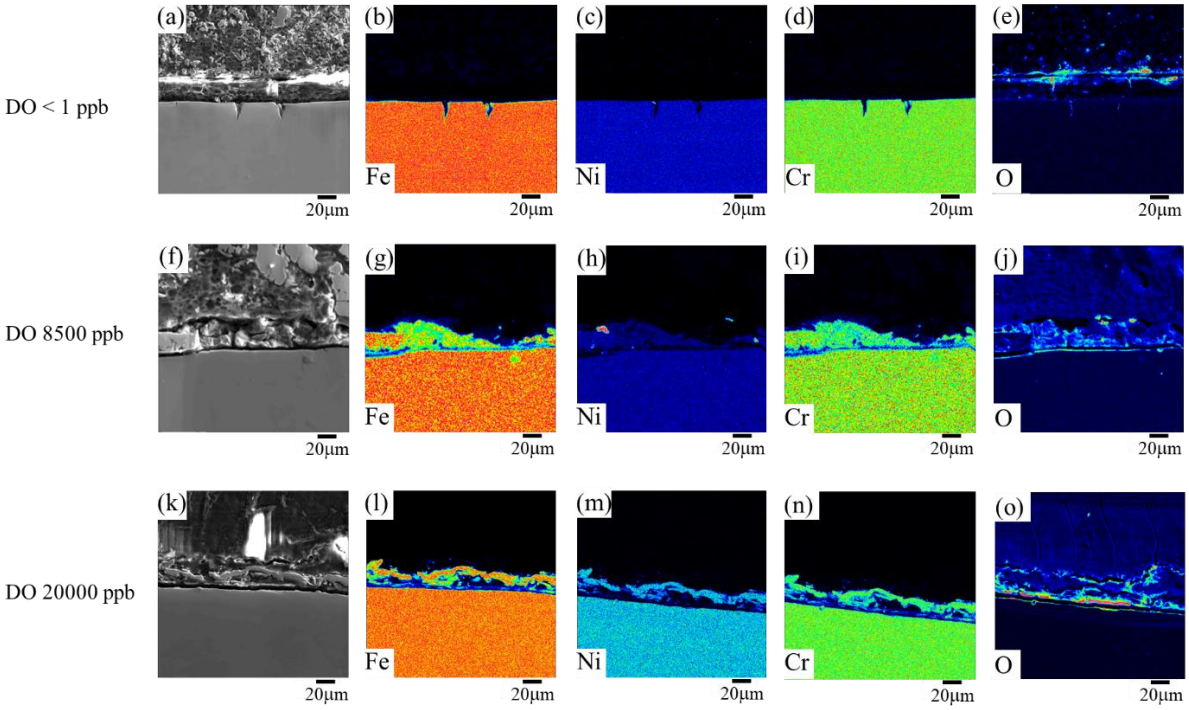

FIGURE 3. EPMA analysis of each element at the surface in the side of the specimen after SSRT with DO change under high temperature pressurized water. (a)Microstructure, (b)Fe, (c)Ni, (d)Cr, (e)O are under DO < 1ppb, (f)Microstructure, (g)Fe, (h)Ni, (i)Cr, (j)O are under DO 8500 ppb, (k) Microstructure, (l)Fe, (m)Ni, (n)Cr, (o)O are under DO 20000 ppb.

surface, and it is assumed that the formation of oxide film suppresses the interaction between (C, Cr) or (C, Ni) solute atomic atmosphere and dislocations. As a result, DSA will be less likely to occur.

3.4. Structural analysis and elemental analysis in the surface layer after SSRT

Figure 4 shows spectral distribution using XPS analysis with narrow scans focused on Fe, Cr, Ni, and O elements after SSRT at DO < 1 ppb and 8500 ppb. At DO < 1 ppb, from the spectral distribution of Fe element, peaks consisting only of Fe and peaks consisting of Fe_3O_4 were observed by fitting. From the spectral distribution of Cr element, it was possible to sort out only the Cr peaks, and no Cr oxide peaks were observed. The spectral distribution of Ni element can also be organized by only the Ni peaks, and no Ni oxide peaks were observed. From the spectral distribution of the O element, peaks of oxygen and metal oxides were observed. In particular, based on the quantitative values of each element derived from these peak distributions, the Cr and Ni concentrations were 17.8 wt% and 7.7 wt%, which were almost similar to the alloy composition of SUS304 itself. In other words, it is indicated that only a small amount of Fe_3O_4 is formed at DO < 1 ppb. On the other hand, at DO 8500 ppb, the peaks of Fe, Fe_3O_4, and FeOOH were observed in contrast to the spectral distribution of only Fe. Furthermore, in addition to the Cr peaks, a blue circle Cr oxide peaks were detected on the right shoulder. The experimental values of Cr and Ni at DO 8500 ppb were 3.59 wt% and 4.06 wt%, respectively, which were significantly lower than the values at DO < 1 ppb. This is indicated that Cr oxides besides Fe were formed in the surface layer due to the increase in oxygen concentration.

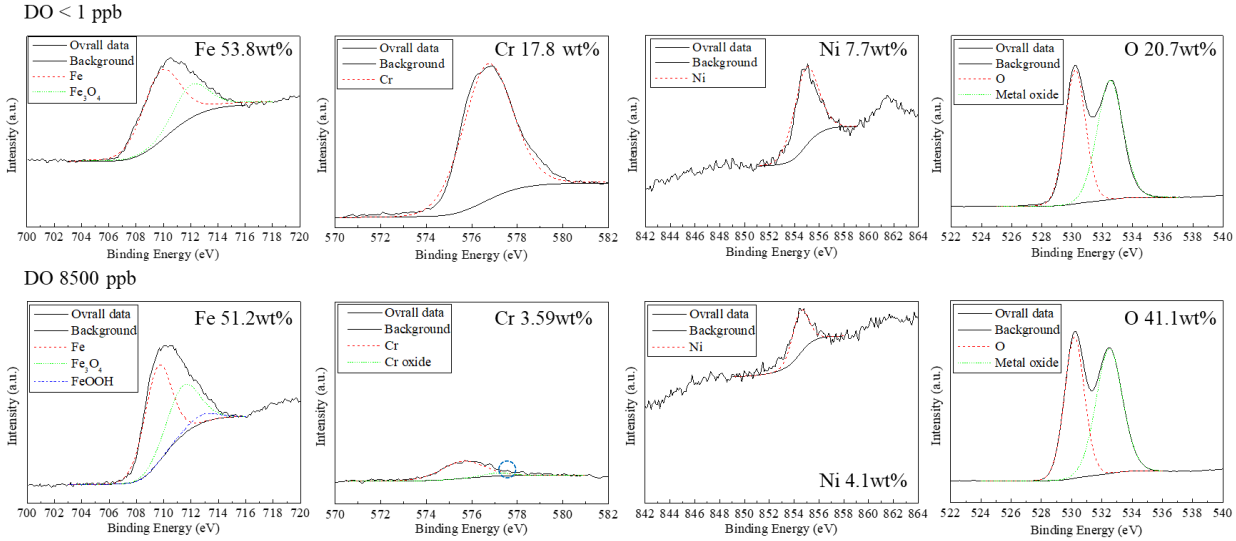

FIGURE 4. Spectral distribution of Fe, Cr, Ni, and O elements using XPS analysis in surface layers after SSRT at DO < 1 ppb and 8500 ppb.

4. DISCUSSIONS

4.1. Mechanisms of DSA and intergranular SCC associated with changes in DO content

The mechanism is discussed here, in which DSA is observed prominently at DO < 1 ppb and 100 ppb, DSA is suppressed at DO 8500 ppb, and at DO 20000 ppb, intergranular SCC with brittle grain boundaries is observed. Figure 5 shows schematically the mechanism of DSA and intergranular SCC at each DO. For DO < 1 ppb and 100 ppb, many intragranular cracks were observed in the side portions after SSRT, and almost no oxide film was formed on the surfaces of these cracks. This result is presumably due to the fact that C element, an interstitial element paired with Cr and Ni elements, adheres to dislocation migration in high temperature environments and under tensile stress. A similar phenomenon was observed in the report by Peng et al. [10], which DSA due to serration occurrence and dislocation entanglement have been reported. On the other hand, since an oxide film of Fe and Cr is formed at DO 8500 ppb, it is assumed that the diffusion of Fe and Cr elements shift to the oxide film side and prevents crack initiation due to pairing with C element. At DO 20000 ppb, O element becomes supersaturated with respect to the oxide film,

and the oxide film peels off from the matrix. O element then begins to diffuse into the grain boundary of the matrix, and it is assumed that the weakening of grain boundary causes intergranular SCC.

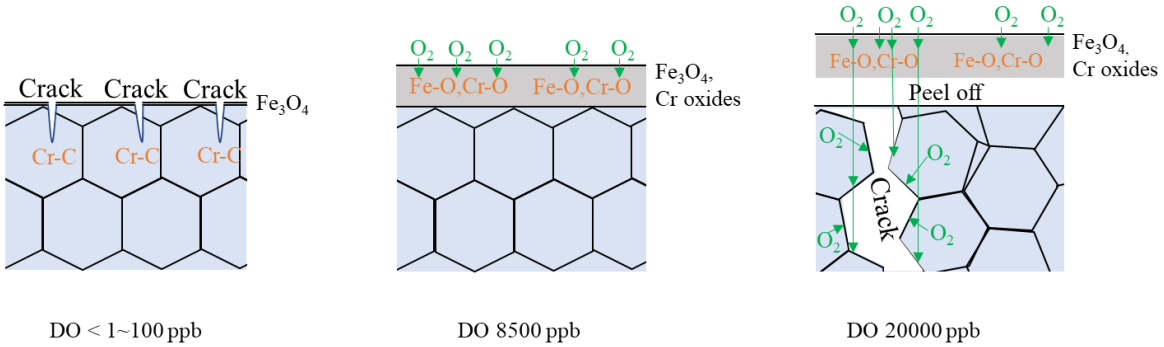

FIGURE 5. Schematic diagram of the mechanism of DSA and intergranular SCC at each DO under high temperature pressurized water.

5. CONCLUSION

The results of this study showed that DSA due to intragranular cracking occurred in SUS304 stainless steel under high temperature pressurized water at DO < 1 ppb and 100 ppb, but at DO 8500 ppb, the occurrence of DSA was suppressed due to the formation of Fe and Cr oxide films on the surface. On the other hand, when DO was further increased to 20000 ppb, the film was peeled from the matrix, and O element diffused into the grain boundary of the matrix, resulting in intergranular SCC. These results are indicated that the optimum DO concentration should be adjusted to suppress crack initiation due to DSA and intergranular SCC.

ACKNOWLEDGMENTS

The authors would like to express their gratitude to Dr. Eitaro Yukitake and Dr. Ryo Ando in the Industrial Technology Innovation Center of Ibaraki Prefecture assisted with specimen preparation and XPS analysis in this study.

REFERENCES

1. Y. Okamura, A. Sakashita, T. Fukuda, H. Yamashita and T. Futami, *Transactions of the 17th International Conference on Structural Mechanics in Reactor Technology (SMiRT 17)*, Czech Republic, 1-10 (2003).
2. J. F. Chen, S. Souma, S. Matsuda and K. Sugimoto, Boshoku Gijutsu, **38**, 203-210 (1989).
3. Y. S. Kim, W. Y. Maeng and S. S. Kim, Acta Mater., **83**, 507–515 (2015).
4. M. Akashi, Boshoku Gijutsu, **29**, 142-151 (1980).
5. K. Kako, Y. Miyahara, K. Hide and M. Mayuzumi, J. Japan Inst. Metals, vol 72, **3**, 206-210 (2008).
6. H. Nakano, T. Uehara, T. Takeuchi, H. Shibata, J. Nakamura, Y. Matsui and K. Tsuchiya, JAEA-Tech., 2015-049, 1-61 (2015).
7. T. Takeuchi, H. Nakano, T. Uehara, K. Tsuchiya, Nucl. Mater. Energy, **9**, 451-454 (2016).
8. M. Okayasu and S. Tomida, Mater. Sci. Eng. A, **684**, 712-725 (2017).
9. P. L. Andresen and M. M. Morra, J. Nucl. Mater., **383**, 97-111 (2008).
10. K. Peng K, K. Qian and W. Chen, Mater. Sci. Eng. A, **379**, 372-377 (2004).